

First measurement of the Hubble parameter from bright binary black hole GW190521

Suvodip Mukherjee^{1*†}, Archisman Ghosh^{1,2,3,4}, Matthew J. Graham⁵,
Christos Karathanasis⁶, Mansi M. Kasliwal⁵, Ignacio Magaña Hernandez⁷,
Samaya M. Nissanke¹, Alessandra Silvestri^{2,3}, Benjamin D. Wandelt^{8,9,10}

¹ *Gravitation Astroparticle Physics Amsterdam (GRAPPA), Anton Pannoeoek Institute for Astronomy and Institute for Physics, University of Amsterdam, Science Park 904, 1090 GL Amsterdam, The Netherlands*

² *Institute Lorentz, Leiden University, PO Box 9506, Leiden 2300 RA, The Netherlands*

³ *Delta Institute for Theoretical Physics, Science Park 904, 1090 GL Amsterdam, The Netherlands*

⁴ *Ghent University, Proeftuinstraat 86, 9000 Gent, Belgium*

⁵ *Division of Physics, Math and Astronomy, California Institute of Technology, 1200 E. California Boulevard, Pasadena, California 91125, USA*

⁶ *Institut de Física d'Altes Energies (IFAE), Barcelona Institute of Science and Technology, Barcelona, Spain*

⁷ *Department of Physics, University of Wisconsin-Milwaukee, Milwaukee, WI 53201, USA*

⁸ *Institut d'Astrophysique de Paris, 98bis Boulevard Arago, 75014 Paris, France*

⁹ *Sorbonne Universites, Institut Lagrange de Paris, 98 bis Boulevard Arago, 75014 Paris, France*

¹⁰ *Center for Computational Astrophysics, Flatiron Institute, 162 5th Avenue, 10010, New York, NY, USA*

1 October 2020

ABSTRACT

The Zwicky Transient Facility (ZTF) reported the event “ZTF19abnrhr” as a candidate electromagnetic (EM) counterpart at a redshift $z = 0.438$ to the gravitational wave (GW) emission from the binary black hole merger GW190521. Assuming that ZTF19abnrhr is the *bona fide* EM counterpart to GW190521, and using the GW luminosity distance estimate from three different waveforms NRSur7dq4, SEOBNRv4PHM, and IMRPhenomPv3HM, we report a measurement of the Hubble constant $H_0 = 50.4^{+28.1}_{-19.5}$ km/s/Mpc, $62.2^{+29.5}_{-19.7}$ km/s/Mpc, and $43.1^{+24.6}_{-11.4}$ km/s/Mpc (median along with 68% credible interval) respectively after marginalizing over matter density Ω_m (or dark energy equation of state w_0) assuming the flat Λ CDM (or w CDM) model. Combining our results with the binary neutron star event GW170817 with its redshift measurement alone, as well as with its inclination angle inferred from Very Large Baseline Interferometry (VLBI), we find $H_0 = 67.6^{+4.3}_{-4.2}$ km/s/Mpc, $\Omega_m = 0.47^{+0.34}_{-0.27}$, and $w_0 = -1.17^{+0.68}_{-0.57}$ (median along with 68% credible interval) providing the most stringent measurement on H_0 and the first constraints on Ω_m and w_0 from bright standard siren. In the future, 1.3% measurement of $H_0 = 68$ km/s/Mpc and 28% measurement of $w_0 = -1$ is possible from about 200 GW190521-like sources.

Key words: Black holes, gravitational wave, cosmology: cosmological parameters

1 INTRODUCTION

Gravitational waves (GWs) from mergers of compact binaries such as neutron stars or black holes have the exquisite property that they give a direct measurement of the luminosity distance to these sources – they are termed as *standard sirens* (Schutz 1986; Holz & Hughes 2005; Dalal et al. 2006;

Nissanke et al. 2010). With additional information on the sources’ redshift z , one can then use the distance-redshift relation $d_l^{GW} = c(1+z) \int_0^z \frac{dz'}{H(z')}$ to measure the cosmological parameters, in particular related to the expansion history $H(z)$, such as the Hubble constant, H_0 , the dark matter density Ω_m , dark energy density Ω_{de} , as well as the equation of state (EoS) of dark energy $w(z) = w_0 + w_a(z/(1+z))$.

Through the last decades, observations of the cosmic microwave background (CMB) (Spergel et al. 2003; Komatsu et al. 2011; Planck Collaboration et al. 2016, 2018), large scale structure (Anderson et al. 2014; Cuesta et al.

* s.mukherjee@uva.nl, mukherje@iap.fr

† The author list is in the alphabetical order except the corresponding author.

2016; Alam et al. 2017), and supernovae (SNe) (Perlmutter et al. 1999; Riess et al. 1996; Freedman & Madore 2010), have gradually established the flat Lambda Cold Dark Matter (LCDM) as the standard model of cosmology. While in this model, the dark energy corresponds to a cosmological constant Λ , with $w = -1$, in general it can be dynamical with a constant, $w(z) = w_0$, (wCDM model) or varying EoS. In recent years, as the different methods to measure this parameter become more and more precise, tensions have started to arise around the value of the Hubble constant H_0 . In particular, early time probes (Planck Collaboration et al. 2016; Abbott et al. 2018; Planck Collaboration et al. 2018) and late time probes (Reid et al. 2009; Riess et al. 2019; Wong et al. 2020; Freedman et al. 2019) are displaying a $4\text{--}5\sigma$ discrepancy in their inferred value for H_0 (Verde et al. 2019).

In this context, GW standard sirens offer an exciting independent probe to measure cosmological parameters, which rely solely on the assumption that General Relativity is correct at astrophysical scales (Schutz 1986). Mergers of binary neutron stars and a subset of neutron star-black hole mergers are expected to result in bright electromagnetic (EM) counterparts which can provide the redshift of the source. The binary neutron star merger GW170817 and associated ultraviolet-optical-infrared counterpart (Abbott et al. 2017c, 2019b) allowed for the identification of the host galaxy NGC4993 (Abbott et al. 2017a,b), and provided us with the first standard siren measurement of $H_0 = 70.3^{+12}_{-8}$ km/s/Mpc (Abbott et al. 2017b; Coulter et al. 2017; Kasliwal et al. 2017). Continued monitoring of the radio afterglow of GW170817 and VLBI measurements (Mooley et al. 2018a) further constrained the viewing angle of the merger and led to improved measurement of $H_0 = 70.3^{+5.3}_{-5.0}$ km/s/Mpc (Hotokezaka et al. 2019). Mergers of stellar-mass binary black holes are usually not expected to have bright EM counterparts unless in significantly gaseous environments, and until recently only the “dark siren” statistical method has been explored to constrain H_0 measurement from such sources, both theoretically (Del Pozzo 2012; Chen et al. 2018; Oguri 2016; Mukherjee & Wandelt 2018; Nair et al. 2018; Gray et al. 2020; Mukherjee et al. 2020; Bera et al. 2020) and empirically (Fishbach et al. 2019; Soares-Santos et al. 2019; Abbott et al. 2019a, 2020b; Palmese et al. 2020). The dark standard siren measurement from the binary black hole (BBH) merger GW170814 is $H_0 = 70^{+40}_{-32}$ km/s/Mpc (Soares-Santos et al. 2019), and that from the recently-reported merger of a black hole with a lighter object GW190814 is $H_0 = 75^{+59}_{-13}$ km/s/Mpc (Abbott et al. 2020b). The current joint measurement with GW170817 along with NGC4993 (no VLBI) and the dark sirens of the first and second observing runs of Advanced LIGO-Virgo (no GW190814) is $H_0 = 68^{+14}_{-7}$ km/s/Mpc (Abbott et al. 2019a).

The Zwicky Transient Facility (ZTF) recently announced a possible EM counterpart, namely an active galactic nucleus (AGN) flare (Graham et al. 2020), in the same sky region at the 78% spatial contour of the GW event GW190521 from the merger of binary black holes (BBHs) observed by the LIGO-Virgo detectors (LIGO Scientific Collaboration et al. 2015; Acernese et al. 2014; Tse et al. 2019; Acernese et al. 2019) on May 21st 2019 at GPS time 1242442967.4473 (Abbott et al. 2020a). ZTF19abnrhr’s

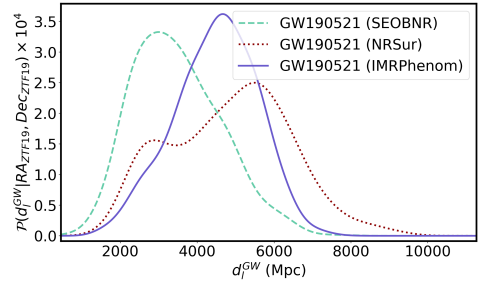


Figure 1. Posterior of the luminosity distance along the sky direction of the EM counterpart ZTF19abnrhr to the GW source GW190521 inferred using three different waveforms (i) SEOBNRv4PHM, (ii) NRSur7dq4, (iii) IMRPhenomPv3HM.

peak luminosity occurred 50 days after the GW trigger which is consistent with predictions of a BBH merger occurring and the remnant being kicked in an AGN disk (McKernan et al. 2019; Yang et al. 2019). The redshift from the ZTF observation together with the low-latency GW localization and distance estimates by LIGO-Virgo makes it possible to measure the expansion history $H(z)$ from the BBH event GW190521 by exploiting the luminosity distance redshift relation. In this Letter, we first describe the data sets which are used for this analysis in Sec. 2, outline briefly our methods and then detail the results of our cosmological parameter constraints for H_0 , matter density Ω_M , and dark energy EoS w_0 in Sec. 3 and Sec. 4 respectively. We conclude in Sec. 5 with a brief discussion of the prospects of such bright GW and EM BBH merger measurements.

2 DATA PRODUCTS USED IN THE ANALYSIS

GW190521: The merger of two black holes each of mass $85^{+21}_{-14} M_\odot$ and $66^{+17}_{-18} M_\odot$ was detected by the Advanced LIGO-Virgo detector network (Tse et al. 2019; Acernese et al. 2019) with a false alarm rate 1 in 4900 years at a luminosity distance $d_l^{GW} = 5.3^{+2.4}_{-2.6}$ Gpc after marginalizing over the sky localisation (Abbott et al. 2020a). The inferred luminosity distance along the direction of the EM counterpart ZTF19abnrhr for analysis with three different GW waveforms (the effective-one-body model SEOBNRv4PHM, the numerical relativity surrogate model NRSur7dq4, and the phenomenological model IMRPhenomPv3HM) are shown in Fig. 1. We also show the posterior distribution along the ZTF direction for the source frame masses, and the inclination angle in Fig. A1 obtained using these three waveforms.

ZTF19abnrhr: ZTF identified a candidate for an EM counterpart to GW190521 at the sky direction ($RA = 192.42625^\circ, Dec = 34.82472^\circ$), dubbed ZTF19abnrhr, which was first observed after 34 days from the GW detection. The candidate EM counterpart was identified in the sky area 78% spatial contour of the GW signal GW190521. The signal is associated with an AGN J124942.3 + 344929 at redshift $z = 0.438$ (Graham et al. 2020).

GW170817: On 17th August 2017, the LIGO and Virgo detectors observed a BNS merger GW170817, which was subsequently observed over the entire EM spectrum (e.g., Kasliwal et al. (2017); Abbott et al. (2017c)). In our analysis, we use the marginalised posterior probability density function (PDF) of H_0 as inferred from the BNS event GW170817 (Abbott et al. 2017a,b), after implementing the peculiar ve-

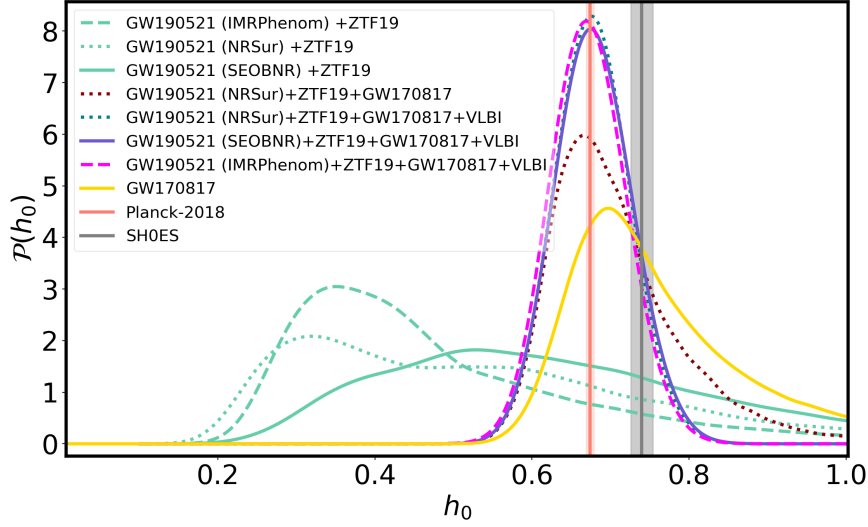


Figure 2. Hubble constant $H_0 = 100 h_0$ km/s/Mpc estimation from GW190521 combining with the ZTF event (in green). We also show the result on H_0 after including GW170817 (in red), and including the VLBI measurement of the inclination angle (in teal, blue, and magenta). For comparison we plot the measured value of $h_0 = 0.674 \pm 0.005$ by the Planck Collaboration et al. (2018) (in salmon), SH0ES team (Riess et al. 2019) $h_0 = 0.74 \pm 0.014$ (in grey), and GW170817 (in yellow) (Abbott et al. 2017a)

locity correction described in Mukherjee et al. (2019). The value of the Hubble constant is $H_0 = 68.3^{+12}_{-7}$ km/s/Mpc with 68% credible intervals.

Inclination angle from the jet of GW170817: The Very Large Baseline Interferometry (VLBI) observations (Mooley et al. 2018a) and the afterglow light curve data (e.g., (Mooley et al. 2018b)) have enabled constraints of the inclination angle i as $0.25 \text{ rad} \leq i \left(\frac{d_L}{11 \text{ Mpc}} \right) \leq 0.45 \text{ rad}$ for GW170817. This, correspondingly, helps place tighter constraints on H_0 ; a revised measurement of Hubble constant is $H_0 = 70.3^{+5.3}_{-5.0}$ km/s/Mpc (Hotokezaka et al. 2019). Implementing the peculiar velocity correction, we find the revised value as $H_0 = 68.3^{+4.6}_{-4.5}$ km/s/Mpc (Mukherjee et al. 2019).

3 METHODS

We compute the posterior distribution for the cosmological parameters $\Theta_c \in \{H_0, \Omega_m, w_0\}$ using the Bayes theorem (Price 1763)

$$\mathcal{P}(\Theta_c | d_l^{GW}, \mathbf{d}_{ZTF}) \propto \int dd_i \mathcal{P}(d_l^{GW} | d_i, \mathbf{d}_{ZTF}, \Theta_c) P(d_i) \Pi(\Theta_c) \quad (1)$$

where d_l^{GW} and \mathbf{d}_{ZTF} are the GW luminosity distance data and ZTF data respectively, $\mathcal{P}(d_l^{GW} | d_i, \mathbf{d}_{ZTF}, \Theta_c)$ is the marginalised probability distribution on the luminosity distance from GW190521. $\Pi(\Theta_c)$ and $\Pi(d_i)$ are the priors on the cosmological parameters and luminosity distance. The detail derivation of the Bayesian framework is given in the Appendix B. We consider uniform ($\Pi(H_0) = \mathcal{U}[10, 150]$, $\Pi(\Omega_m) = \mathcal{U}[0.1, 1]$, $\Pi(w_0) = \mathcal{U}[-2, -0.1]$). In this analysis, we obtain the results for two models (i) LCDM model with $\Theta_c \in \{H_0, \Omega_m\}$ (keeping $w_0 = -1$ fixed), and (ii) wCDM model with $\Theta_c \in \{H_0, w_0\}$ (keeping $\Omega_m = 0.315$ (Planck Collaboration et al. 2018)). The joint estimation of the cosmological parameters Ω_m (or w_0) and H_0 are important as the source is situated at high redshift. The results are obtained for three different combinations of data sets (see Sec. 2 for the details) (D1) GW190521+ZTF19abarrhr, (D2) GW190521+ZTF19abarrhr+GW170817, (D3) GW190521+ZTF19abarrhr+GW170817+VLBI, each for

three different choices of GW waveforms (a) SEOBNRv4PHM, (b) NRSur7dq4, (c) IMRPhenomPv3HM¹.

4 RESULTS

Constraints on Hubble constant H_0 : After marginalizing over Ω_m , the posterior of H_0 for D1a, D1b, and D1c are shown in Fig. 2. The mild differences in the luminosity distance posteriors inferred using three different waveforms IMRPhenomPv3HM, NRSur7dq4, and SEOBNRv4PHM, leads to the observed difference in the Hubble constant posterior, as can be seen from the dashed, dotted, and solid lines in green. The median value of the Hubble constant for data sets D1a, D1b, and D1c with 68% credible interval are $H_0 = 62.2^{+29.5}_{-19.7}$ km/s/Mpc, $H_0 = 50.4^{+28.1}_{-19.5}$ km/s/Mpc, and $H_0 = 43.1^{+24.6}_{-11.4}$ km/s/Mpc respectively. The differences in the value of the Hubble constant from different methods are not statistically significant. After combining with the measurement from GW170817, the median value of the Hubble constant for D2b becomes $H_0 = 69.1^{+9.4}_{-5.8}$ km/s/Mpc as shown by the dark-red colour in Fig. 2². This improves the constraints in the higher values of H_0 . Inclusion of the VLBI measurement provides the most stringent measurement from GW observations $H_0 = 67.6^{+4.3}_{-4.2}$ km/s/Mpc as shown in Fig. 2 for D3b. The results for D3a and D3c are $H_0 = 67.7^{+4.6}_{-4.2}$ km/s/Mpc and $H_0 = 67.1^{+4.4}_{-4.2}$ km/s/Mpc respectively which are consistent with the result from D3b. The measurement with the data sets D3b is in agreement with the best-fit value of $H_0 = 67.4 \pm 0.5$ km/s/Mpc from the Planck collaboration (Planck Collaboration et al. 2016, 2018) and is about 1.6σ (assuming a Gaussian distribution) away from the SH0ES value of $H_0 = 74. \pm 1.4$ km/s/Mpc (Riess et al. 2019).

¹ Hereafter we denote a particular combination of data set such as GW190521 (SEOBNRv4PHM) +ZTF19abarrhr as “D1a”.

² We have chosen the waveform NRSur7dq4 than the other waveforms as it is calibrated with the numerical simulations.

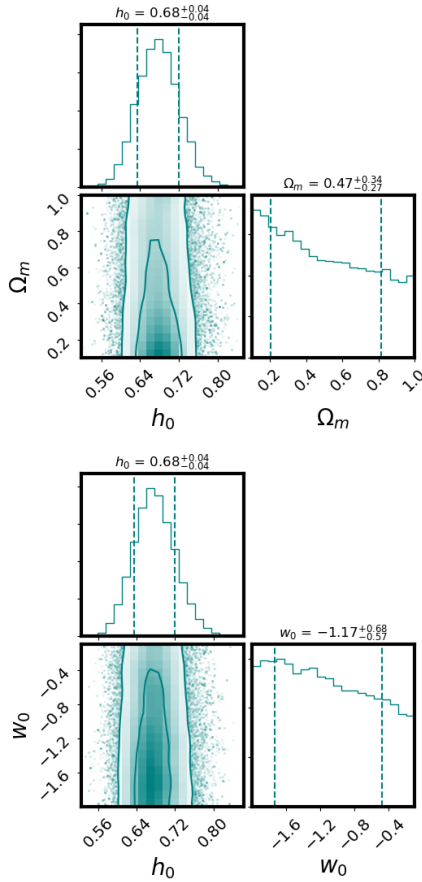


Figure 3. The joint estimation of the Hubble constant $H_0 = 100h_0$ km/s/Mpc and (i) Ω_m with a fixed value of dark energy EoS $w_0 = -1$ and (ii) w_0 with fixed $\Omega_m = 0.315$ for the combination of data sets D3b.

Constraints on Ω_m and w_0 : For the combination of datasets D3b, we show the joint parameter estimation $H_0 + \Omega_m$ (for the LCDM model) and $H_0 + w_0$ (for the wCDM model) in Fig. 3. The mean value and the 68% credible interval of the matter density and dark energy EoS are $\Omega_m = 0.47^{+0.34}_{-0.27}$ and $w_0 = -1.17^{+0.68}_{-0.57}$ respectively. Though the constraints are weak, this provides the first estimation on matter density and dark energy EoS using standard sirens allowing slightly lower values. The bounds for the combination of data sets D3a and, D3c are also similar. With an increase in the number of GW sources, even in the absence of EM counterparts, the cosmological parameters Ω_m and $w(z)$ will also be measured accurately from the LIGO/Virgo detectors (Mukherjee et al. 2020).

5 CONCLUSION AND FUTURE OUTLOOK

We present here the measurement of the Hubble constant $H_0 = 50.4^{+28.1}_{-19.5}$ km/s/Mpc from bright standard siren GW190521 using the waveform NRSur7dq4, after marginalizing over matter density Ω_m for the LCDM model of cosmology. This is the first measurement of the Hubble constant from a BBH merger having its candidate EM counterpart detected by ZTF (Graham et al. 2020). By combining the results from the BNS event GW170817 along with the constraints on the inclination angle from VLBI, we report the most stringent measurement of Hubble constant $H_0 = 67.6^{+4.3}_{-4.2}$ km/s/Mpc from standard sirens. Using GW190521, we are able to obtain constraints on the matter density

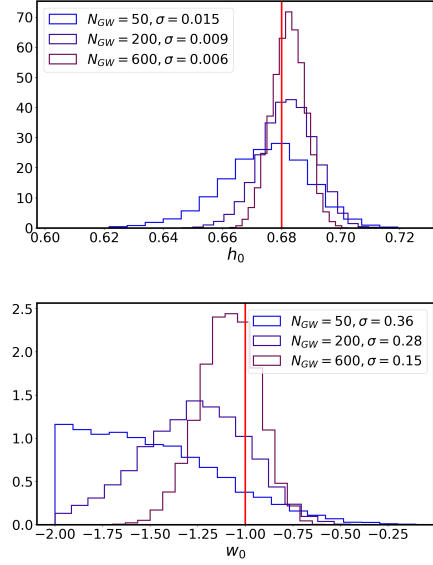


Figure 4. Forecast: The posterior distribution on h_0 , w_0 possible from GW190521-like sources detectable up to redshift $z = 1$ with EM counterpart, with individual masses $85 M_\odot$ and $66 M_\odot$ in the source-frame. The line in red shows the injected value.

$\Omega_m = 0.47^{+0.34}_{-0.27}$ and dark energy EoS $w_0 = -1.17^{+0.68}_{-0.57}$ for the first time from standard sirens. Other independent analysis are also carried out adding the prior from Planck (Chen et al. 2020) and using GW waveforms including eccentricity Gayathri et al. (2020).

Future measurements with N_{GW} BBHs with identified EM counterparts, can expect to beat the statistical uncertainty by $N_{GW}^{-1/2}$. Using BBHs similar to the source-frame masses of the event GW190521 ($m_1 = 85 M_\odot$, $m_2 = 66 M_\odot$), we estimate the measurability of the cosmological parameters at LIGO/Virgo design sensitivity (Acernese et al. 2014; Abbott et al. 2016). Considering the GW sources distributed up to redshift $z = 1$ for which electromagnetic counterparts can be detected by ZTF, we show the posterior distribution on $H_0 = 100h_0$ km/s/Mpc, and w_0 in Fig. 4. This shows that our method can reliably recover the injected value of the cosmological parameters with an uncertainty about 1.3% on H_0 and with about 28% on $w_0 = -1$ from 200 GW sources.

In summary, the redshift measurement of GW190521 opens a new paradigm of measurements with multi-messenger cosmology using BBHs. Accurate identification of EM counterparts from BBHs will allow not only to measure the expansion history up to high redshift but also to explore different aspects of fundamental physics. This avenue is going to be useful also for the future space-based GW detector Laser Interferometer Space Antenna (LISA) (Amaro-Seoane et al. 2017). LISA will detect super-massive BBHs which are also likely to have EM counterparts in gas-rich environments (Armitage & Natarajan 2002; Palenzuela et al. 2010; Farris et al. 2015; Haiman 2018), and this observation of an EM candidate is possibly the first step towards the detection of EM counterparts on BBHs in gas-rich environments.

AVAILABILITY OF DATA

The datasets were derived from sources in the public domain: <https://dcc.ligo.org/LIGO-P2000158/public>.

ACKNOWLEDGEMENT

We thank Simone Mastrogiovanni for carefully reviewing the manuscript and providing useful suggestions. SM acknowledges useful discussions with Will M. Farr and Rachel Gray. This analysis was carried out at the Horizon cluster hosted by IAP. We thank Stephane Rouberol for smoothly running the Horizon cluster. SM and SMN are supported by the research program Innovational Research Incentives Scheme (Vernieuwingsimpuls), which is financed by the Netherlands Organization for Scientific Research through the NWO VIDI Grant No. 2016/ENW/639.042.612. AG is grateful for funding from the D-ITP. This work was supported by the GROWTH project funded by the National Science Foundation under Grant No 1545949. This work was partially supported by the Spanish MINECO under the grants SEV-2016-0588 and PGC2018-101858-B-I00, some of which include ERDF funds from the European Union. IFAE is partially funded by the CERCA program of the Generalitat de Catalunya. IMH is supported by the NSF Graduate Research Fellowship Program under grant DGE-17247915. AS acknowledges support from the NWO and the Dutch Ministry of Education, Culture and Science (OCW) (through NWO VIDI Grant No. 2019/ENW/00678104 and from the D-ITP consortium). BDW and part of the computational work are supported by the Labex ILP (reference ANR-10-LABX-63) part of the IDEX SUPER, received financial state aid managed by the Agence Nationale de la Recherche, as part of the programme Investissements d'avenir under the reference ANR-11-IDEX-0004-02. BDW acknowledges financial support from the ANR BIG4 project, under reference ANR-16-CE23-0002. The Center for Computational Astrophysics is supported by the Simons Foundation. In this analysis, following packages are used: Corner (Foreman-Mackey 2016), emcee: The MCMC Hammer (Foreman-Mackey et al. 2013), IPython (Pérez & Granger 2007), Matplotlib (Hunter 2007), NumPy (van der Walt et al. 2011), and SciPy (Jones et al. 01).

REFERENCES

- Abbott B. P., et al., 2016, *Phys. Rev. D*, 93, 112004
 Abbott B. P., et al., 2017a, *Phys. Rev. Lett.*, 119, 161101
 Abbott B. P., et al., 2017b, *Nature*, 551, 85
 Abbott B., et al., 2017c, *Astrophys. J. Lett.*, 848, L12
 Abbott T., et al., 2018, *Mon. Not. Roy. Astron. Soc.*, 480, 3879
 Abbott B., et al., 2019a, arXiv:1908.06060
 Abbott B. P., et al., 2019b, *Phys. Rev. X*, 9, 011001
 Abbott R., et al., 2020a, *Phys. Rev. Lett.*, 125, 101102
 Abbott R., et al., 2020b, *Astrophys. J.*, 896, L44
 Acernese F., et al., 2014, *Classical and Quantum Gravity*, 32, 024001
 Acernese F., et al., 2019, *Phys. Rev. Lett.*, 123, 231108
 Alam S., et al., 2017, *Mon. Not. Roy. Astron. Soc.*, 470, 2617
 Amaro-Seoane P., et al., 2017, arXiv e-prints, p. arXiv:1702.00786
 Anderson L., et al., 2014, *Mon. Not. Roy. Astron. Soc.*, 441, 24
 Armitage P. J., Natarajan P., 2002, *Astrophys. J.*, 567, L9
 Bera S., Rana D., More S., Bose S., 2020, arXiv:2007.04271
 Chen H.-Y., Fishbach M., Holz D. E., 2018, *Nature*, 562, 545
 Chen H., et al., 2020, Under preparation
 Coulter D., et al., 2017, *Science*, 358, 1556
 Cuesta A. J., et al., 2016, *Mon. Not. Roy. Astron. Soc.*, 457, 1770
 Dalal N., Holz D. E., Hughes S. A., Jain B., 2006, *Phys. Rev. D*, 74, 063006
 Del Pozzo W., 2012, *Phys. Rev. D*, 86, 043011
 Farr W. M., Gair J. R., October 2018, <https://github.com/farr/H0StatisticalLikelihood/blob/master-pdf/h0stat.pdf>,
 Farris B. D., Duffell P., MacFadyen A. I., Haiman Z., 2015, *Mon. Not. Roy. Astron. Soc.*, 447, L80
 Feeney S. M., et al., 2019, *Phys. Rev. Lett.*, 122, 061105
 Fishbach M., et al., 2019, *Astrophys. J. Lett.*, 871, L13
 Foreman-Mackey D., 2016, *The Journal of Open Source Software*, 24
 Foreman-Mackey D., Hogg D. W., Lang D., Goodman J., 2013, *PASP*, 125, 306
 Freedman W. L., Madore B. F., 2010, *ARA&A*, 48, 673
 Freedman W. L., et al., 2019, *ApJ*, 882, 34
 Gayathri V., et al., 2020, Under preparation
 Graham M. J., et al., 2020, *Phys. Rev. Lett.*, 124, 251102
 Gray R., et al., 2020, *Phys. Rev. D*, 101, 122001
 Haiman Z., 2018, *Found. Phys.*, 48, 1430
 Holz D. E., Hughes S. A., 2005, *ApJ*, 629, 15
 Hotokezaka K., Nakar E., Gottlieb O., Nissanke S., Masuda K., Hallinan G., Mooley K. P., Deller A., 2019, *Nature Astron.*
 Hunter J. D., 2007, *Computing In Science & Engineering*, 9, 90
 Jones E., Oliphant T., Peterson P., et al., 2001–, SciPy: Open source scientific tools for Python,
 Kasliwal M., et al., 2017, *Science*, 358, 1559
 Komatsu E., et al., 2011, *ApJS*, 192, 18
 LIGO Scientific Collaboration et al., 2015, *Classical and Quantum Gravity*, 32, 074001
 McKernan B., et al., 2019, *Astrophys. J. Lett.*, 884, L50
 Mooley K. P., et al., 2018a, *Nature*, 561, 355
 Mooley K. P., et al., 2018b, *ApJL*, 868, L11
 Mortlock D. J., et al., 2019, *Phys. Rev. D*, 100, 103523
 Mukherjee S., Wandelt B. D., 2018, arXiv:1808.06615
 Mukherjee S., et al., 2019, arXiv:1909.08627
 Mukherjee S., et al., 2020, arXiv:2007.02943
 Nair R., Bose S., Saini T. D., 2018, *Phys. Rev. D*, 98, 023502
 Nicolaou C., et al., 2020, *Mon. Not. Roy. Astron. Soc.*, 495, 90
 Nissanke S., Holz D. E., Hughes S. A., Dalal N., Sievers J. L., 2010, *ApJ*, 725, 496
 Oguri M., 2016, *Phys. Rev. D*, 93, 083511
 Palenzuela C., Lehner L., Liebling S. L., 2010, *Science*, 329, 927
 Palmese A., et al., 2020, *Astrophys. J.*, 900, L33
 Pérez F., Granger B. E., 2007, *Computing in Science and Engineering*, 9, 21
 Perlmutter S., et al., 1999, *Astrophys. J.*, 517, 565
 Planck Collaboration et al., 2016, *A&A*, 594, A13
 Planck Collaboration et al., 2018, arXiv e-prints, p. arXiv:1807.06209
 Price T. B., cited January 1763, LII. An essay towards solving a problem in the doctrine of chances. By the late Rev. Mr. Bayes
 Reid M. J., Braatz J. A., Condon J. J., Greenhill L. J., Henkel C., Lo K. Y., 2009, *ApJ*, 695, 287
 Riess A. G., Press W. H., Kirshner R. P., 1996, *Astrophys. J.*, 473, 88
 Riess A. G., Casertano S., Yuan W., Macri L. M., Scolnic D., 2019, *Astrophys. J.*, 876, 85
 Schutz B. F., 1986, *Nature*, 323, 310
 Soares-Santos M., et al., 2019, *Astrophys. J. Lett.*, 876, L7
 Spergel D., et al., 2003, *Astrophys. J. Suppl.*, 148, 175
 Tse M., et al., 2019, *Phys. Rev. Lett.*, 123, 231107
 Verde L., Treu T., Riess A., 2019. (arXiv:1907.10625), doi:10.1038/s41550-019-0902-0
 Wong K. C., et al., 2020, *MNRAS*,
 Yang Y., et al., 2019, *Phys. Rev. Lett.*, 123, 181101
 van der Walt S., Colbert S. C., Varoquaux G., 2011, *Computing in Science and Engineering*, 13, 22

APPENDIX A: GW SOURCE PROPERTIES ALONG THE SKY DIRECTION ZTF19ABANRHR

The posterior distributions for GW source masses (m_1 and m_2) and inclination angle i along the line of sight of ZTF event are shown in Figs. A1 for the three waveform models (i) SEOBNR, (ii) NRSur, and (iii) IMRPhenomPv3HM. These distributions have been obtained by re-weighting the samples of the LIGO-Virgo data release with a Gaussian prior on the sky centered at the location of ZTF19abanrhr with an effective beam size of 10 sq. deg. The mass distributions show a bimodality for all the three waveforms, which is most explicit for NRSur. The inclination angle shows slightly higher probability towards the values $i < 90^\circ$.

APPENDIX B: BRIEF DISCUSSION OF THE BAYESIAN FRAMEWORK RELEVANT FOR THE ANALYSIS OF GW SOURCES WITH EM COUNTERPART

Let us consider a GW source detected with matched-filter signal to noise ratio $\rho > \rho_*$, where ρ_* is the detection threshold. For this event, we have identified the EM counterparts within some time interval Δt in the sky area identified from the GW observation. Using Bayes theorem (Price 1763), we can write the probability distribution of the EM data vector \mathbf{d}_{EM} which includes its redshift \hat{z} and sky location $(\hat{\theta}, \hat{\phi})$ given an observed EM counterpart \mathcal{O}_{EM} , galaxy catalog g containing the spectroscopically measured redshift, and astrophysical model I_A of the source as

$$\begin{aligned} \mathcal{P}(\mathbf{d}_{EM}|d_{GW}, g, I_A) &\propto \Pi(\hat{z}, \hat{\theta}, \hat{\phi}) \int d\Delta t \int d\Omega_{sky} \quad (\text{B1}) \\ &\times P(g|\mathcal{O}_{EM}(t + \Delta t), z, \theta, \phi) P(\mathcal{O}_{EM}(t + \Delta t)|d_{GW}(t), I_A) \\ &\times P(\Delta t|I_A) \end{aligned}$$

where, $\Pi(\hat{z}, \hat{\theta}, \hat{\phi})$ is the prior on the redshift of the source \hat{z} , and its sky direction $(\hat{\theta}, \hat{\phi})$, $P(g|\mathcal{O}_{EM}(t + \Delta t), z, \theta, \phi)$ is the likelihood of the EM data vector given galaxy catalog and EM counterpart \mathcal{O}_{EM} , $P(\mathcal{O}_{EM}(t + \Delta t)|d_{GW}(t), I_A)$ is the likelihood of the EM counterpart given GW data d_{GW} and astrophysical model I_A , $P(\Delta t|I_A)$ is the probability that the signal is observed after time Δt from GW observation for a given model I_A . The posterior given in Eq. B1 is not normalised, but this does not affect cosmological parameter inference.

The association of the GW signal and EM signal are made by observing both the signals in the time-domain. With the aid of the time-domain aspect, we can relate the redshift space information with the luminosity distance space information for a single GW source. When such association is absent, one needs to estimate the prior $P_{pop}(z, \theta, \phi|\Omega_c)$ of the allowed redshift values for a given choice of cosmological parameters Ω_c and assuming redshift distribution of the GW merger rates. If a pair of EM and GW signal is identified ($\mathcal{P}(\mathbf{d}_{EM}|d_{GW}, g, I_A)$ using Eq. B1), then there is no need to choose the prior $P_{pop}(z, \theta, \phi|\Omega_c)$ on the allowed redshift and sky positions separately for a choice of cosmological parameters with an assumption on the population. One can use $\mathcal{P}(\mathbf{d}_{EM}|d_{GW}, g, I_A)$ as the prior on the redshift and sky location.

We will explain this aspect in more details with a

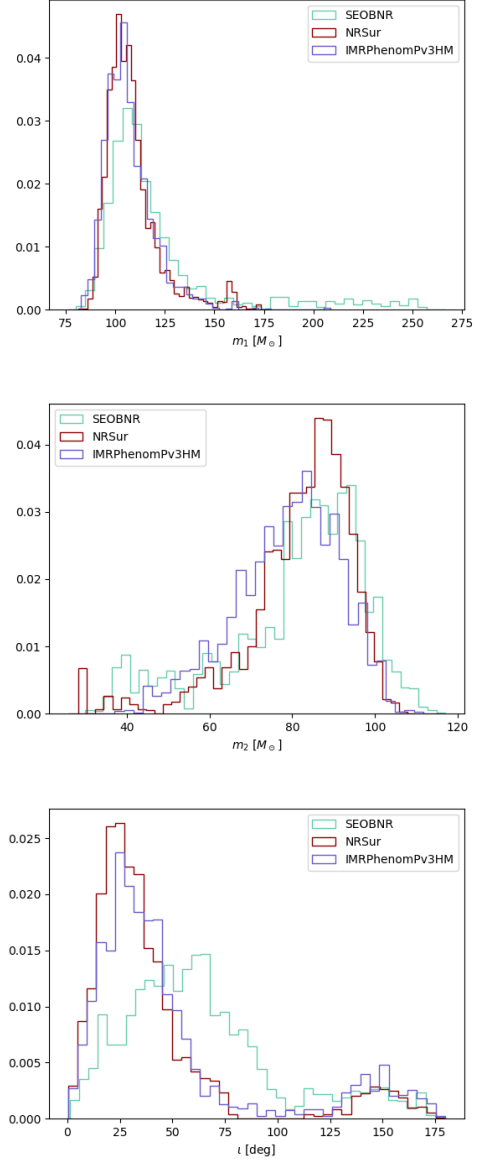


Figure A1. We show the posterior distribution on the mass m_1 of the heavier component BH, m_2 of the lighter component BH in the source frame, and the inclination angle along the sky direction of the EM counterpart ZTF19abanrhr inferred using three different waveforms (i) SEOBNRv4PHM, (ii) NRSur7dq4, (iii) IMRPhenomPv3HM.

schematic diagram given in Fig. B1 which shows the luminosity distance d_l and redshift z plane for the case with EM counterpart (top) and case without EM counterpart (bottom). In the presence of an EM counterpart, one has a measurement of the redshift \hat{z} (shown in blue) and the corresponding luminosity distance \hat{d}_l^{GW} (shown in magenta). The combination of both these leads to estimate the best-fit cosmological parameters by fitting the luminosity distance and redshift relation, which are plotted for different choices cosmological parameters in different colors. The horizons for GW and EM observations which are shown by the red line and black line sets the maximum luminosity distance d_{max} and maximum redshift z_{max} accessible from GW detectors

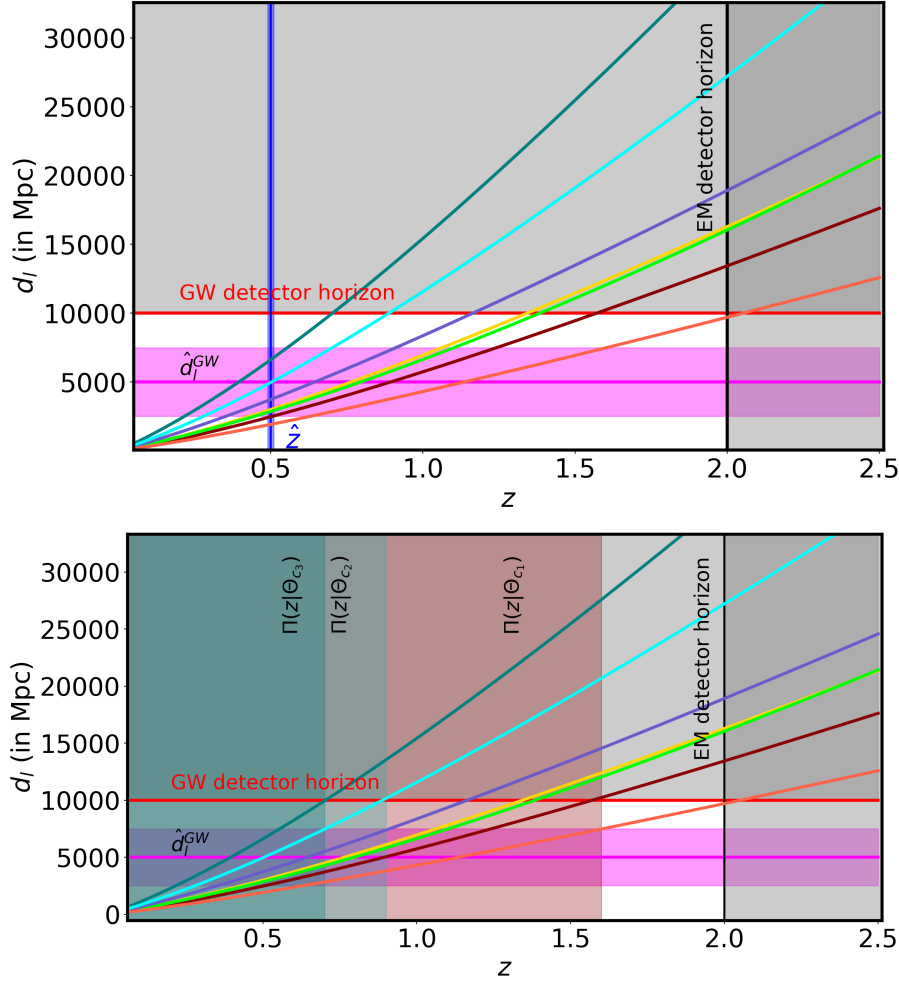


Figure B1. Schematic diagrams showing the two scenarios with EM counterpart (top) and without EM counterpart (bottom). We plot the luminosity distance d_l and redshift z plane for different cosmological models by different colors. The line in red shows the GW horizon in luminosity distance d_{max} for a given GW detector noise and GW parameters in the detector-frame. For this schematic diagram, we have assumed $d_{max} = 10$ Gpc. The line in black indicates the horizon for an EM follow-up instrument, which is assumed to be redshift $z = 2$. The region shaded in grey above and right-side of the red and black line respectively are inaccessible to the GW and EM detectors. The region in magenta shows the luminosity distance \hat{d}_l^{GW} inferred from a GW observation with the corresponding $1 - \sigma$ error bar by the shaded region. In the top plot, we show the corresponding redshift \hat{z} identified from EM follow-up in blue. In the bottom panel, we show the priors $\Pi(z, \Theta_{c_i})$ on redshift one needs to choose in the absence of an EM counterpart for different choices of the cosmological parameters Θ_{c_i} . Different shaded regions in teal, cyan and red color extend from $z = 0$ to $z_{max} = z(d_{max}, \Theta_{c_i})$ which corresponds to the different parameter choices Θ_{c_i} (the corresponding distances are plotted in the same colors). The change in the maximum allowed redshift values with the change in cosmological parameters, for a fixed d_{max} makes the priors depend on cosmology.

and EM detectors respectively³. So, the region not shaded in grey is the total accessible region in the luminosity distance redshift plane.

In the bottom panel we show the case when there is no EM counterpart. Here, one needs to choose a prior on the redshift $\Pi(z, \Theta_{c_i})$. Even for a fixed value of d_{max} , this prior depends on the cosmological parameters Θ_{c_i} as shown by the shaded regions in teal, cyan and red which corresponds to the maximum redshift $z_{max} = z(d_{max}, \Theta_{c_i})$ (for any cosmo-

logical model (shown in different colors) z_{max} is the redshift where the luminosity distance redshift curve intersects the maximum luminosity distance d_{max}). So, depending on the choice of the cosmological parameters the range of allowed redshift varies. The total accessible parameter space is a combination of the allowed prior on redshift z and luminosity distance d_{max} , which is also cosmology dependent. As a result, it is important to also include the probability associated with the population of the GW sources and its merger rates to the corresponding redshifts which are allowed by the prior. This is because for certain choices of the cosmological parameters, the value of z_{max} can be large enough that the GW sources of stellar-origin are unlikely to be produced.

³ EM observations will also have a cutoff in luminosity distance. But for this schematic diagram, we have assumed that it is much larger than d_{max} .

However, when EM counterpart is present, such choices regarding the population are not required, as the association of a pair of GW and EM signal and the corresponding association of the luminosity distance d_l^{jGW} and redshift \hat{z} pair are made using the time-domain information under the assumption of an astrophysical model I_A , as shown in Eq. B1. Under an extremely rare scenario, if one identifies two EM counterpart originating from two different redshift within the same sky patch of the GW signal. Then one can use the population-based model to associate higher probability of being the EM counterpart to one of the events over the other.

The EM counterpart gives a measurement of the redshift \hat{z} , and sky directions $\hat{\theta}, \hat{\phi}$. We assume that the EM data is accurately known. By using the luminosity distance $d_l(z, \Theta_c)$ and redshift z relation, we can obtain the cosmological parameters Θ_c using the Bayes theorem, which can be written as

$$\begin{aligned} \mathcal{P}(\Theta_c | d_{GW}, \mathbf{d}_{EM}, I_A) &\equiv \mathcal{P}(\Theta_c | d_{GW}, \mathbf{d}_{EM}) \propto \frac{\Pi(\Theta_c)}{\beta(\Theta_c)} \quad (\text{B2}) \\ &\times \int d\Theta_{GW} \int dd_l P(d_{GW} | d_l, \Theta_c, \mathbf{d}_{EM}, \Theta_{GW}) P(\Theta_{GW} | \mathbf{d}_{EM}) \\ &\quad \times P(d_l), \end{aligned}$$

where $\Pi(\Theta_c)$ is the prior on the cosmological parameters $\Theta_c \in \{H_0, \Omega_m, w_0, w_a\}$, $P(d_{GW} | d_l, \Theta_c, \mathbf{d}_{EM}, \Theta_{GW})$ is the likelihood given the EM data, $P(\Theta_{GW} | \mathbf{d}_{EM})$ is the probability distribution of the GW source parameters $\Theta_{GW} \in \{M_z, i, \Omega_{sky}\}$ (such as detector frame mass M_z , inclination angle i , sky solid angle Ω_{sky}), given the EM data set. This is useful in converting the detector-frame mass M_z to the source-frame mass $M = M_z / (1 + \hat{z})$, understanding about the inclination angle i using the EM observation such as the astrophysical jet (Mooley et al. 2018a; Mooley et al. 2018b), and identifying the sky localization of the GW source using the sky direction of the EM counterpart. $P(d_l)$ is the prior on the luminosity distance. After marginalizing over the GW source parameters Θ_{GW} , we can simplify Eq. B2 as

$$\mathcal{P}(\Theta_c | d_{GW}, \mathbf{d}_{EM}) \propto \frac{\Pi(\Theta_c)}{\beta(\Theta_c)} \int dd_l P(d_{GW} | d_l, \mathbf{d}_{EM}, \Theta_c) P(d_l), \quad (\text{B3})$$

where d_{GW} is the luminosity distance marginalised over all the GW source parameters for the fixed redshift \hat{z} , and sky direction $\hat{\theta}, \hat{\phi}$ available from \mathbf{d}_{EM} . The normalization factor $\beta(\Theta_c)$ can be written as

$$\begin{aligned} \beta(\Theta_c) &= \int d\Theta_{GW} \int d_{GW} \int \mathbf{d}_{EM} \int dd_l P(d_{GW} | d_l, \theta, \phi, \Theta_{GW}) \\ &\quad \times P(\Theta_{GW} | \mathbf{d}_{EM}) P(d_l). \end{aligned} \quad (\text{B4})$$

Assuming the EM counterparts are detected up to a maximum redshift z_{max} with isotropic sensitivity in all directions and similarly, the GW sources are detected up to a maximum luminosity distance $d_{max}(\theta, \phi, \Theta_{GW})$. So, we can write $P(d_{GW} | d_l(\hat{z}, \Theta_c), \theta, \phi, \Theta_{GW}) = \mathcal{H}(d_{max}(\theta, \phi, \Theta_{GW}) - d_l)^4$. Then Eq. B4 becomes

$$\begin{aligned} \beta(\Theta_c) &= \int d\Theta_{GW} \int dd_l \int d_{GW} \int \mathbf{d}_{EM} P(\Theta_{GW} | \mathbf{d}_{EM}) \\ &\quad \times \mathcal{H}(d_{max}(\theta, \phi, \Theta_{GW}) - d_l) P(d_l), \\ &= \int d\Theta_{GW} \int_0^{d_{max}(\theta, \phi, \Theta_{GW})} dd_l P(\Theta_{GW}) P(d_l), \\ &= \text{constant}. \end{aligned} \quad (\text{B5})$$

The above integration is independent of the cosmological

parameters and depends only on the maximum value of the luminosity distance d_{max} and maximum redshift z_{max} , similar to the conclusion obtained by previous analysis (Abbott et al. 2017b; Farr & Gair 2018). So, we can ignore this in the overall normalization in the Eq. B3. In the Bayesian formalism mentioned in Eq. B2, we have not included the correction due to the peculiar velocity, as it is not relevant for the source GW190521. However, previous studies have elaborately discussed the Bayesian formalism for the peculiar velocity correction of GW sources (Abbott et al. 2017b; Feeney et al. 2019; Mortlock et al. 2019; Mukherjee et al. 2019; Nicolaou et al. 2020) which can be easily incorporated in Eq. B2.

⁴ $\mathcal{H}(x)$ is the Heaviside step function.